ChemComm

Chemical Communications

rsc.li/chemcomm

ROYAL SOCIETY
OF CHEMISTRY
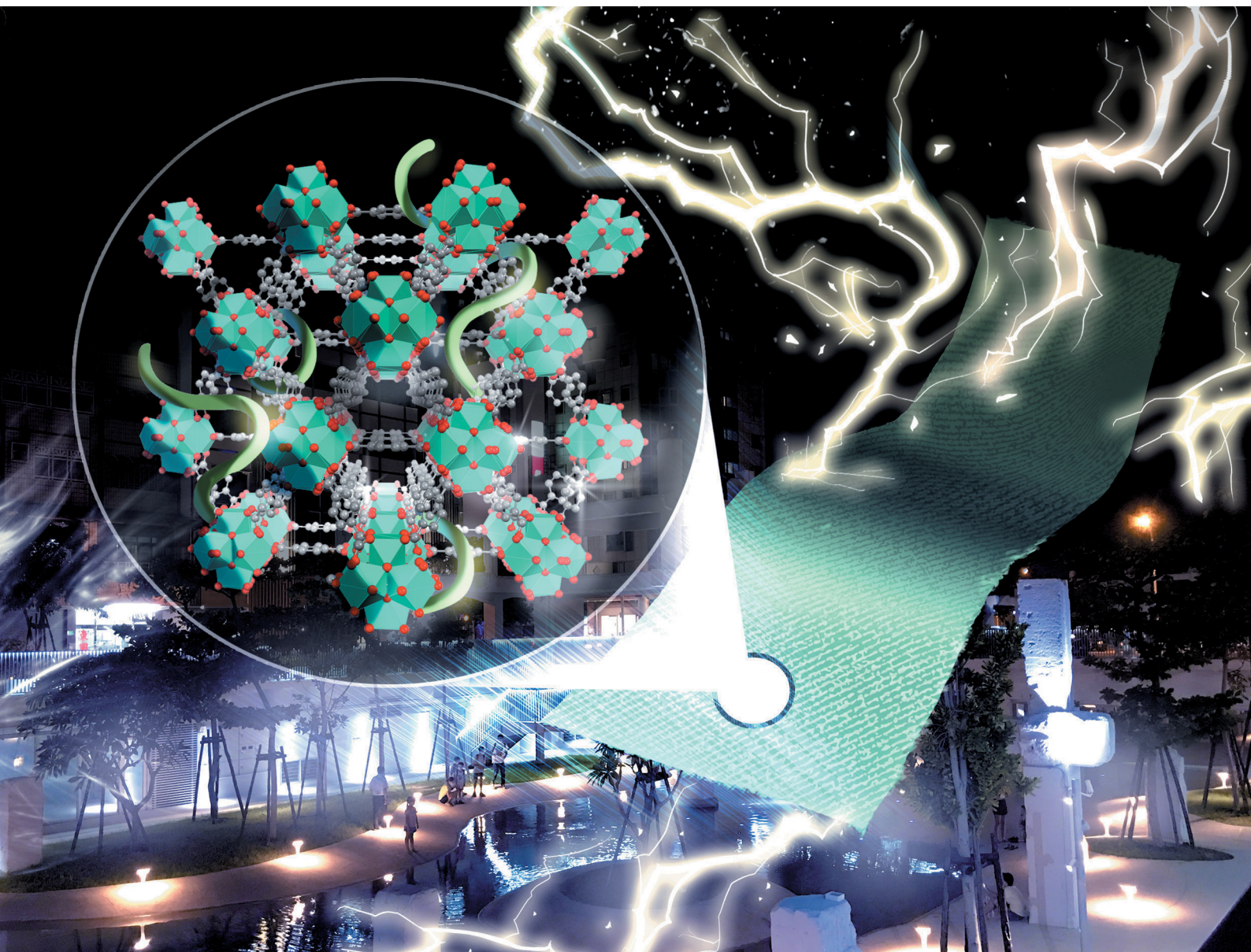
COMMUNICATION
Bekir Satilmis, Chung-Wei Kung *et al.*
Metal–organic framework functionalized poly-cyclodextrin
membranes confining polyaniline for charge storage

Check for updates

Metal–organic framework functionalized poly-cyclodextrin membranes confining polyaniline for charge storage†

Ramachandran Rajakumaran,[a] Cheng-Hui Shen,[a] Bekir Satilmis [ID] *[ab] and Chung-Wei Kung [ID] *[a]

Crystals of a metal–organic framework, UiO-66, are grown on electrospun crosslinked poly-cyclodextrin (poly-CD) fibrous membranes with an ultrahigh coverage, and polyaniline (PANI) is further confined within the MOF pores. The obtained PANI@UiO-66/poly-CD membranes are used as free-standing electrodes towards use in wearable energy-storage devices.

Metal–organic frameworks (MOFs)[1,2] have attracted significant attention in recent years and have been applied for a range of applications due to their exceptionally high specific surface area, interconnected porosity, and tuneable pore size with versatile functionalities.[3–6] For example, MOF-derived metal oxides and relevant inorganic materials have been widely used in supercapacitors.[7–9] The major concern that limits the direct applications of most pristine MOFs is their poor stability in water, but the development of highly stable group 4 metal-based MOFs, *e.g.*, zirconium-based MOFs (Zr-MOFs), has allowed the use of MOFs in aqueous or humid environments without damaging their structures.[10,11] Such chemically robust and highly porous Zr-MOFs are thus considered as attractive materials for several electrochemical applications because of their highly accessible internal surface areas with built-in electrochemically active sites that may be capable of electrocatalysis or charge storage.[12–16]

In addition to utilizing the pristine Zr-MOFs with electrochemical activity in such applications, another material-design route is using Zr-MOFs as a rigid template to confine the electrochemically active species within interconnected pores in order to increase their accessible surface area. For example,

polyaniline (PANI), a commonly used conducting polymer that can be used in electrochemical sensors and charge storage,[17] could be synthesized in the presence of Zr-MOFs due to the structural integrity of Zr-MOFs in the acidic aqueous solutions required for the polymerisation of aniline (ANI).[18–21] The resulting electrochemical performances of such PANI@ Zr-MOF composites are usually better than those of the pristine PANI.[19,20] Very recently, for the first time, we developed a unique approach to selectively generate continuous PANI confined within the pores of a Zr-MOF, while preventing the formation of PANI solid between MOF crystals.[22] Such a pore-confined PANI in a Zr-MOF was also found to outperform the pristine PANI as the active material for electrochemical capacitors.[22]

Cyclodextrins (CDs) consist of toroid-shaped cyclic oligosaccharides with α(1,4)-linked D-glucopyranose units. CDs contain a hydrophobic core owing to –CH and –CH$_2$ carbons and a hydrophilic exterior surface resulting from multiple hydroxyl groups.[23] Electrospinning CD molecules could be achieved without the necessity of carrier polymers, but their high solubility in an aqueous environment limits their use in various applications.[24] Recently, crosslinked poly-CDs have been introduced to overcome this limitation and employed in water treatment applications.[25,26] These crosslinked poly-CD fibrous membranes could also be an ideal platform for the growth of MOF crystals owing to the rich hydroxyl groups that may effectively initiate the nucleation of carboxylate-based MOFs. However, to date there is no study reporting the growth of MOFs on poly-CD yet.

Herein, nanocrystals of a Zr-MOF, UiO-66,[27] were grown on the electrospun free-standing membranes consisting of poly-CD fibres with an ultrahigh surface coverage. As a demonstration, the obtained UiO-66/poly-CD membranes were further subjected to the spatially selective polymerisation of ANI to generate continuous PANI confined within the pores of grown MOF crystals (Fig. 1). The flexible and free-standing electrodes with remarkable and stable electrochemical activity in aqueous

[a] Department of Chemical Engineering, National Cheng Kung University, 1 University Road, Tainan City, 70101, Taiwan. E-mail: cwkung@mail.ncku.edu.tw

[b] Department of Medical Services and Techniques, Vocational School of Health Services, Kirsehir Ahi Evran University, Kirsehir, 40100, Turkey. E-mail: bekir.satilmis@ahievran.edu.tr
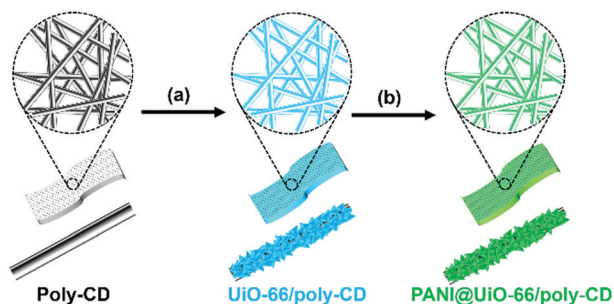
Fig. 1 Scheme for the (a) growth of UiO-66 nanocrystals on the free-standing membrane of poly-CD fibres and (b) the spatially selective polymerisation of ANI to generate the continuous PANI confined within the MOF crystals.

electrolytes can thus be obtained, which are highly desirable for the future design of wearable electrochemical devices.

The electrospun membranes composed of poly-CD fibres were prepared by following the procedure reported previously,[25] and UiO-66 nanocrystals were thereafter grown on poly-CD through a room-temperature process.[28,29] The membrane of UiO-66/poly-CD was thus obtained (see detailed experimental procedure in the ESI†). As shown in Fig. 2(a) and (b), the free-standing and flat membrane can still be obtained even after the growth of UiO-66 and the subsequent washing, solvent-exchange, and drying processes. Scanning electron microscopic (SEM) images of the pristine poly-CD and UiO-66/poly-CD are shown in Fig. 2(f) and (g), respectively, which reveals the even and full coverage of the octahedral MOF crystals on the surface of all the poly-CD fibres. The ultrahigh coverage of the grown UiO-66 nanocrystals can be viewed in low-magnification SEM images of the membranes as well (see Fig. S2, ESI†). This observation implies that the rich terminal hydroxyl groups present on the surface of the poly-CD fibres should allow effective nucleation for growing MOF crystals

from the surface, which results in the high coverage of MOF nanocrystals on the surface of the poly-CD fibres.

UiO-66/poly-CD was thereafter used as the platform for the polymerisation of ANI with the addition of excessive poly(sodium 4-styrenesulfonate) (PSS). Under such polymerisation conditions, a well-dispersed PANI:PSS polymer solution without precipitation can be formed.[22] However, since PSS is more bulky compared to the MOF pore, only the ANI monomer and initiator can penetrate into the nanopores of UiO-66 to generate the pore-confined PANI solid. Therefore, by successively washing the resulting membrane with HCl solutions to fully remove the residual PANI:PSS, PANI confined within the UiO-66 nanocrystals grown on poly-CD (PANI@UiO-66/poly-CD) can be obtained; see the detailed experimental procedure in the ESI.† A similar strategy has been used to prepare pore-confined PANI in the powder of another Zr-MOF recently.[22] As displayed in Fig. 2(c), the free-standing and flat characteristics of the membrane are still preserved after the polymerisation, and the colour of the membrane becomes green. Except for the slightly rougher surface of the MOF crystals, no obvious morphological changes can be observed after the polymerisation, as revealed in the SEM images shown in Fig. 2(h) and (i). This finding suggests that no obvious bulk PANI or PANI:PSS is present outside the MOF crystals; this observation agrees well with that for powder samples reported in recent work.[22] Elemental mapping data also show the uniform distributions of Zr, O, N and C on the fibres (Fig. S3, ESI†). For comparison, the pristine poly-CD membrane was also subjected to the same polymerisation process. As shown in Fig. S4 (ESI†), PANI solid with a dark green colour can still be formed and immobilized near the edge of the poly-CD membrane, but the structure of the membrane got completely destroyed after the drying process, which results in a fragile and non-uniform material. This preliminary assessment indicates that the presence of uniformly grown UiO-66 crystals may also
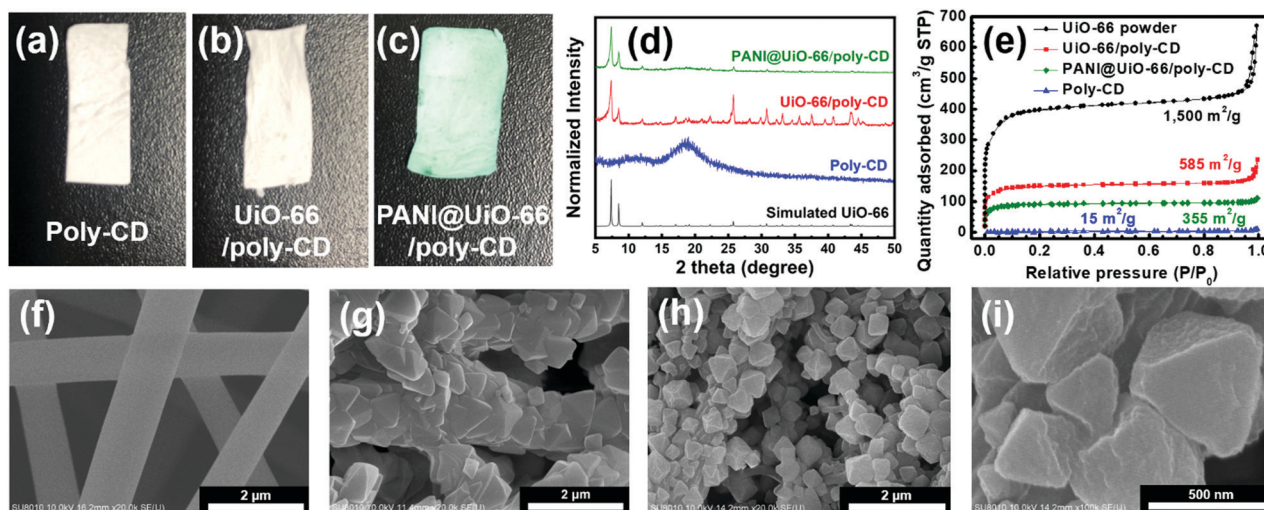

Fig. 2 Photos of (a) poly-CD, (b) UiO-66/poly-CD, and (c) PANI@UiO-66/poly-CD. (d) GIXRD patterns of the membranes. (e) Nitrogen adsorption-desorption isotherms and obtained BET surface areas of the membranes and UiO-66 powder. SEM images of (f) poly-CD, (g) UiO-66/poly-CD, and (h) PANI@UiO-66/poly-CD. (i) High-magnification SEM image of PANI@UiO-66/poly-CD.

play an important role in providing the poly-CD membrane with a better mechanical stability required for the polymerisation of ANI in such membranes.

Grazing incidence X-ray diffraction (GIXRD) patterns of the membranes are present in Fig. 2(d). All the main diffraction peaks appearing in the patterns of UiO-66/poly-CD and PANI@UiO-66/poly-CD are consistent with those shown in the simulated pattern of UiO-66, which indicates that the phase-pure and crystalline UiO-66 can be grown on the poly-CD membrane, and the crystallinity of UiO-66 is well preserved after the incorporation of PANI. It should be noticed that the pattern of poly-CD possesses a wide and broad amorphous peak located at around 20 degree, which also agrees with that observed for poly-CD reported in a previous work.[30] Nitrogen adsorption-desorption measurements were then performed to examine the porosity of all membranes, and the data are plotted in Fig. 2(e). In comparison with the pristine MOF powder with a Brunauer–Emmett–Teller (BET) surface area of 1500 $m^2 g^{-1}$, UiO-66/poly-CD shows an obviously decreased BET surface area of 585 $m^2 g^{-1}$, and this value further drops to 355 $m^2 g^{-1}$ after the incorporation of PANI. The pristine poly-CD shows a negligible porosity (15 $m^2 g^{-1}$). The typical microporous characteristic of UiO-66 can be seen in the isotherms of both UiO-66/poly-CD and PANI@UiO-66/poly-CD, suggesting that the microporosity of UiO-66 can be partially preserved in both membranes. Density functional theory (DFT) pore size distributions were further extracted from the isotherms in Fig. 2(e), and the data are shown in Fig. S5 (ESI†). All the UiO-66 powder, UiO-66/poly-CD, and PANI@UiO-66/poly-CD possess a pore size between 1 nm and 2 nm, which in general matches the characteristics of defective UiO-66 synthesized by a similar procedure.[28] It should be noticed that after the incorporation of PANI, the pore volume of UiO-66/poly-CD between 1.6 and 1.9 nm, the pore size corresponding to the defective cavity of UiO-66,[28] decreases significantly. This finding indicates that PANI is mainly confined within the defective cavity of UiO-66 crystals grown on the membrane; this observation is also consistent with our previous finding for powder samples.[22]

Fourier-transform infrared spectroscopy (FTIR) was employed to further characterize the membranes, and the data are shown in Fig. S6 (ESI†). Detailed discussion is provided in the ESI.† The characteristic peaks of poly-CD appear in the FTIR spectra of all the poly-CD, UiO-66/poly-CD, and PANI@UiO-66/poly-CD, and the peaks of PANI are present in the FTIR spectrum of PANI@UiO-66/poly-CD. This result again suggests the successful formation of PANI in the membrane. Thermogravimetric analysis (TGA) was further performed, and the results suggest that the mass fraction of MOF in UiO-66/poly-CD is 21.6%, and the mass fraction of polyaniline in PANI@UiO-66/poly-CD is 25.8% (see detailed discussion regarding Fig. S7 in the ESI†).

Cyclic voltammetric (CV) curves of the membranes were first tested at 100 mV s^{-1} in an aqueous electrolyte containing 0.2 M of HCl to examine the electrochemical behaviours of the membranes. As shown in Fig. 3(a), the electrodes with
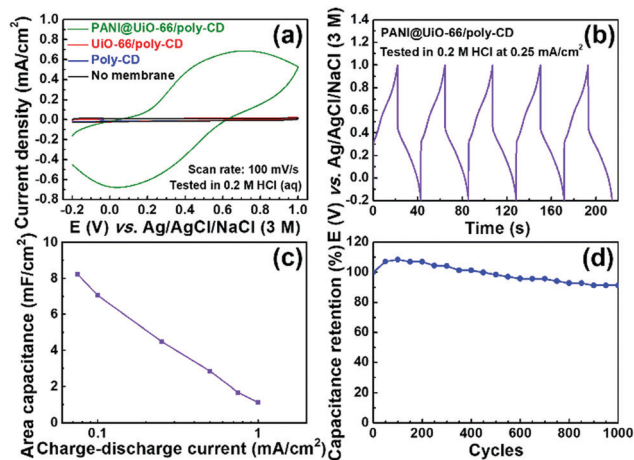

Fig. 3 (a) CV data of poly-CD, UiO-66/poly-CD, PANI@UiO-66/poly-CD, and the electrode without a membrane, measured at 100 mV s^{-1}. (b) Five-cycle GCD curve of PANI@UiO-66/poly-CD collected at 0.25 mA cm^{-2}. (c) Capacity of PANI@UiO-66/poly-CD measured at each charge–discharge rate. (d) Capacitance retention of PANI@UiO-66/poly-CD during the GCD processes at 0.5 mA cm^{-2} for 1000 cycles.

poly-CD and UiO-66/poly-CD do not exhibit any electrochemical activity, and the non-faradaic current in their CV curves is almost the same as that of the bare electrode (see the zoom-in CV curves in Fig. S8, ESI†). On the other hand, the CV curve of PANI@UiO-66/poly-CD reveals one set of broad redox peaks, with the anodic peak and cathodic peak centred at 0.71 V and 0.03 V vs. Ag/AgCl/NaCl (3 M), respectively. CV curves of PANI@UiO-66/poly-CD were thereafter measured at different scan rates (v), and as revealed in Fig. S9(a) (ESI†), two sets of redox peaks appear at slower v within this potential window. This electrochemical feature is consistent with that typically reported for PANI in acidic aqueous electrolytes,[31] which suggests that the Zr-MOF-confined PANI grown on the membrane is electrochemically active. Values of anodic peak current density (J_{pa}) and cathodic peak current density (J_{pc}) were further extracted from the CV curves, and the plots of log(J_{pa}) vs. log(v) and log($|J_{pc}|$) vs. log(v) are shown in Fig. S9(b) and (c) (ESI†), respectively. Slopes of 0.65 and 0.59 were obtained from these plots, respectively, indicating that the electrochemical reactions occurring on PANI@UiO-66/poly-CD are more similar to a diffusion-controlled process rather than the process of a surface-mounted electroactive monolayer.[32] Slopes here also imply that the pore-confined PANI shows a characteristic between those of ideal capacitive materials and materials for batteries, with a higher similarity to a battery-type material.[33]

Chronopotentiometric experiments were thereafter conducted to probe the charge–storage capability of PANI@UiO-66/poly-CD. As shown in Fig. 3(b), the membrane can be reversibly charged and discharged at 0.25 mA cm^{-2}. Galvanostatic charge–discharge (GCD) curves of all membranes were also measured at different current densities (J_{cd}). As shown in Fig. S10 (ESI†), both the poly-CD and UiO-66/poly-CD possess negligible capacities. Obvious changes in slope can be observed in the GCD curves of PANI@UiO-66/poly-CD, especially at small

J_{cd}; this feature is consistent with the typical characteristic of a pseudocapacitive material.[33] By utilizing the discharged time in each curve, the area capacitance at each J_{cd} was estimated, and the values are plotted in Fig. 3(c). The area capacitance reaches 8.2 mF cm^{-2} when a J_{cd} of 0.075 mA cm^{-2} is applied. An impedance study was also performed (see discussion regarding Fig. S11 in the ESI†). A long-term charge–discharge experiment was then conducted for the PANI@UiO-66/poly-CD membrane electrode (Fig. 3(d) and Fig. S12, ESI†). Except for the slightly increased capacitance during the first 100 cycles, presumably owing to the swelling of PANI during the electrochemical process,[22] the capacitance of PANI@UiO-66/poly-CD is fairly stable during 1000 cycles of the GCD process at a J_{cd} of 0.5 mA cm^{-2}; the area capacitance is still 91% of that achieved during the first cycle after 1000 cycles of the GCD process. The comparison between PANI@UiO-66/poly-CD and some reported MOF-based capacitive materials is shown in Table S1 (ESI†).

In summary, UiO-66 nanocrystals can be grown on the membrane composed of poly-CD fibres with a high coverage, and the subsequent polymerisation of ANI in an HCl solution can be performed within the grown MOF crystals. The UiO-66 crystals not only provide the nanopores for the formation of high-surface-area pore-confined PANI, but also enhance the mechanical stability of the membrane. The resulting membrane of PANI@UiO-66/poly-CD can be used as a free-standing electrode in aqueous HCl electrolytes towards use in supercapacitors. Ongoing work is focused on the use of water-stable MOF/poly-CD membranes for other applications like separation as well as the development of such electrically conductive MOF-based fibrous membranes for wearable energy-storage devices.

Conflicts of interest

There are no conflicts to declare.

References

1 H. Furukawa, K. E. Cordova, M. O'Keeffe and O. M. Yaghi, *Science*, 2013, **341**, 1230444.
2 H.-C. J. Zhou and S. Kitagawa, *Chem. Soc. Rev.*, 2014, **43**, 5415–5418.
3 Z. R. Herm, E. D. Bloch and J. R. Long, *Chem. Mater.*, 2014, **26**, 323–338.
4 M. B. Majewski, A. W. Peters, M. R. Wasielewski, J. T. Hupp and O. K. Farha, *ACS Energy Lett.*, 2018, **3**, 598–611.
5 C. Wang, J. Kim, J. Tang, M. Kim, H. Lim, V. Malgras, J. You, Q. Xu, J. Li and Y. Yamauchi, *Chem*, 2020, **6**, 19–40.
6 S. Jeoung, S. Kim, M. Kim and H. R. Moon, *Coord. Chem. Rev.*, 2020, **420**, 213377.
7 J. Pan, S. Li, F. Li, T. Yu, Y. Liu, L. Zhang, L. Ma, M. Sun and X. Tian, *Colloids Surf., A*, 2021, **609**, 125650.
8 J. Pan, S. Li, L. Zhang, T. Yu, F. Li, W. Zhang, J. Wang, D. Zhang, Y. Yu and X. Li, *J. Energy Storage*, 2022, **47**, 103550.
9 J. Pan, S. Li, F. Li, W. Zhang, D. Guo, L. Zhang, D. Zhang, H. Pan, Y. Zhang and Y. Ruan, *J. Alloys Compd.*, 2022, **890**, 161781.
10 S. Yuan, J.-S. Qin, C. T. Lollar and H.-C. Zhou, *ACS Cent. Sci.*, 2018, **4**, 440–450.
11 A. J. Howarth, Y. Liu, P. Li, Z. Li, T. C. Wang, J. T. Hupp and O. K. Farha, *Nat. Rev. Mater.*, 2016, **1**, 15018.
12 C.-W. Kung, S. Goswami, I. Hod, T. C. Wang, J. Duan, O. K. Farha and J. T. Hupp, *Acc. Chem. Res.*, 2020, **53**, 1187–1195.
13 S. Lin, Y. Pineda-Galvan, W. A. Maza, C. C. Epley, J. Zhu, M. C. Kessinger, Y. Pushkar and A. J. Morris, *ChemSusChem*, 2017, **10**, 514–522.
14 J.-H. Li, Y.-S. Wang, Y.-C. Chen and C.-W. Kung, *Appl. Sci.*, 2019, **9**, 2427.
15 B. A. Johnson, A. Bhunia, H. Fei, S. M. Cohen and S. Ott, *J. Am. Chem. Soc.*, 2018, **140**, 2985–2994.
16 K. M. Choi, H. M. Jeong, J. H. Park, Y.-B. Zhang, J. K. Kang and O. M. Yaghi, *ACS Nano*, 2014, **8**, 7451–7457.
17 C. O. Baker, X. Huang, W. Nelson and R. B. Kaner, *Chem. Soc. Rev.*, 2017, **46**, 1510–1525.
18 C.-C. Lin, Y.-C. Huang, M. Usman, W.-H. Chao, W.-K. Lin, T.-T. Luo, W.-T. Whang, C.-H. Chen and K.-L. Lu, *ACS Appl. Mater. Interfaces*, 2019, **11**, 3400–3406.
19 L. Shao, Q. Wang, Z. Ma, Z. Ji, X. Wang, D. Song, Y. Liu and N. Wang, *J. Power Sources*, 2018, **379**, 350–361.
20 Y. Wang, L. Wang, W. Huang, T. Zhang, X. Hu, J. A. Perman and S. Ma, *J. Mater. Chem. A*, 2017, **5**, 8385–8393.
21 J. Shanahan, D. S. Kissel and E. Sullivan, *ACS Omega*, 2020, **5**, 6395–6404.
22 Y.-D. Song, W. H. Ho, Y.-C. Chen, J.-H. Li, Y.-S. Wang, Y.-J. Gu, C.-H. Chuang and C.-W. Kung, *Chem. – Eur. J.*, 2021, **27**, 3560–3567.
23 A. Dodero, G. Schlatter, A. Hébraud, S. Vicini and M. Castellano, *Carbohydr. Polym.*, 2021, **264**, 118042.
24 A. Celebioglu and T. Uyar, *Langmuir*, 2011, **27**, 6218–6226.
25 A. Celebioglu, Z. I. Yildiz and T. Uyar, *Sci. Rep.*, 2017, **7**, 7369.
26 A. Celebioglu, F. Topuz, Z. I. Yildiz and T. Uyar, *ACS Omega*, 2019, **4**, 7850–7860.
27 J. H. Cavka, S. Jakobsen, U. Olsbye, N. Guillou, C. Lamberti, S. Bordiga and K. P. Lillerud, *J. Am. Chem. Soc.*, 2008, **130**, 13850–13851.
28 M. R. DeStefano, T. Islamoglu, S. J. Garibay, J. T. Hupp and O. K. Farha, *Chem. Mater.*, 2017, **29**, 1357–1361.
29 C.-H. Chuang, J.-H. Li, Y.-C. Chen, Y.-S. Wang and C.-W. Kung, *J. Phys. Chem. C*, 2020, **124**, 20854–20863.
30 D. Han, Z. Han, L. Liu, Y. Wang, S. Xin, H. Zhang and Z. Yu, *Int. J. Mol. Sci.*, 2020, **21**, 766.
31 X. L. Wei, Y. Z. Wang, S. M. Long, C. Bobeczko and A. J. Epstein, *J. Am. Chem. Soc.*, 1996, **118**, 2545–2555.
32 A. J. Bard and L. R. Faulkner, *Electrochemical methods, fundamentals and applications*, John Wiley & Sons, New York, 2001.
33 Y. Jiang and J. Liu, *Energy Environ. Mater.*, 2019, **2**, 30–37.